Quantitative Magnetic Resonance Spectroscopy in the Entire Human Cervical Spinal Cord and Beyond at 3T

Anke Henning,[1*] Michael Schär,[1] Spyros S. Kollias,[2] Peter Boesiger,[1] and Ulrike Dydak[1]

Quantitative magnetic resonance spectroscopy (MRS) amends differential diagnostics of neurological pathology. However, due to technical challenges, it has rarely been applied to the spinal cord and has mainly been restricted to the very upper part of the cervical spine. In this work, an improved acquisition protocol is proposed that takes technical problems as strong magnetic field inhomogeneities, pulsatile flow of the cerebrospinal fluid (CSF), and small voxel size into account. For that purpose, inner-volume saturated point-resolved spectroscopy sequence (PRESS) localization, ECG triggering, and localized higher-order shimming and F_0 determination, based on high-resolution cardiac-triggered static magnetic field B_0 mapping, are combined. For inner-volume saturation a highly selective T_1- and B_1-insensitive outer-volume suppression (OVS) sequence based on broadband RF pulses with polynomial-phase response (PPR) is used. Validation is performed in healthy volunteers and patients with multiple sclerosis and intramedullary tumors. The applicability of spinal cord MRS is extended to the entire cervical spine. Spectral quality and its consistency are improved. In addition, high quality MRS patient data from a lesion that occluded the spinal canal in the thoracic spinal cord could be acquired. A quantitative analysis of patient spectra and spectra from healthy volunteers at different positions along the spinal cord underlines the diagnostic value of spinal cord MRS. Magn Reson Med 59:1250–1258, 2008. © 2008 Wiley-Liss, Inc.

Key words: MRS; cervical; thoracic; spinal cord; outer-volume suppression; B_0 map; shim; CSF; pulsatile flow

Magnetic resonance spectroscopy (MRS) noninvasively provides information on the biochemistry of neuronal tissue which is complementary to conventional MRI investigations. Concentration changes of metabolites such as N-acetyl-aspartate (NAA), choline containing compounds (Cho), creatine (Cre), or myo-inositol (mI) indicate decreased neuronal density or neuronal dysfunction, such as decreased neurotransmitter excretion, distorted membrane synthesis, malfunction of the energy metabolism, or demyelination, respectively. Specific patterns of metabolic changes observable by MRS point toward certain disorders of the central nervous system such as multiple sclerosis, low- and high-grade tumors, amyotrophic lateral sclerosis, or spino-cerebellar ataxia. Hence, MRS aids in the differential diagnosis of space-occupying lesions and various metabolic diseases. Therefore, investigation of human brain pathology by quantitative MRS has gained increased acceptance by clinicians (1).

However, due to technical challenges, quantitative spinal cord MRS has rarely been used and was mainly restricted to the brain stem and the upper part of the cervical spine down to the C2-C3 level (2–6). Preliminary studies indicate that metabolite concentrations are sufficiently high to be observed by MRS in the entire spinal cord, but spectral quality was insufficient for quantification in the middle and lower cervical and even more in the thoracic and lumbar spinal cord (7–9). Susceptibility differences between vertebral bodies, intervertebral discs, and the surrounding tissue lead to strong magnetic field inhomogeneities (2). The pulsatile flow of the cerebrospinal fluid (CSF) induced by cardiac and respiratory motion causes phase fluctuations, water suppression failure, and movement of the spinal cord. F_0 misdetermination leads to dislocation of the spectroscopy voxel and, therefore, to lipid contamination arising from epidural, muscular, and subcutaneous fat, and bony marrow. The chemical shift displacement artifact, caused by bandwidth limitations of slice-selective excitation and refocusing pulses, limits the signal-to-noise ratio (SNR) due to imprecise localization and anomalous J-modulation (10) and induces ghosting artifacts (11) due to the inclusion of CSF into the voxel as well as lipid contamination.

In this work, the applicability of quantitative MR spectroscopy is expanded to larger segments of the spinal cord. Furthermore, the spectral quality and its consistency is improved. To that, an enhanced acquisition sequence is proposed that takes the above mentioned technical problems into account. The use of inner-volume saturated point-resolved spectroscopy (PRESS) (10) aims at precise localization, CSF flow artifact reduction, and avoidance of lipid contamination. To that a T_1- and B_1-insensitive outer-volume suppression (OVS) (12) based on highly selective, broadband saturation pulses with polynomial-phase response (PPR) (13) is utilized. Localized higher-order shimming and F_0 determination, based on high-resolution cardiac-triggered static magnetic field B_0 mapping (14), aims at reduction of static magnetic field inhomogeneities and avoidance of dislocation of the spectroscopy volume. To obviate motion artifacts and to enhance shimming ECG triggering is applied (2).

[1]Institute for Biomedical Engineering, University and Federal Institute of Technology (ETH) Zurich, Switzerland.

[2]Neuroradiology, University Hospital Zurich, Switzerland

Grant sponsors: Philips Medical Systems (Best, the Netherlands); National Centers of Competence in Research (NCCR) on Neural Plasticity and Repair (Switzerland).

Current affiliations for Michael Schär: Philips Medical Systems, Cleveland, Ohio, USA; Russell H. Morgan Department of Radiology and Radiological Science, Johns Hopkins University, Baltimore, Maryland, USA.

Current affiliations for Ulrike Dydak: School of Health Sciences, Purdue University, West Lafayette, Indiana, USA; Division of Imaging Sciences, Department of Radiology, Indiana University School of Medicine, Indianapolis, Indiana, USA.

*Correspondence to: Anke Henning, Institute for Biomedical Engineering, University and ETH Zurich, Gloriastrasse 35, CH-8092 Zurich, Switzerland. E-mail: henning@biomed.ee.ethz.ch

Received 10 June 2007; revised 5 December 2007; accepted 8 January 2008.

DOI 10.1002/mrm.21578

Published online in Wiley InterScience (www.interscience.wiley.com).

© 2008 Wiley-Liss, Inc.

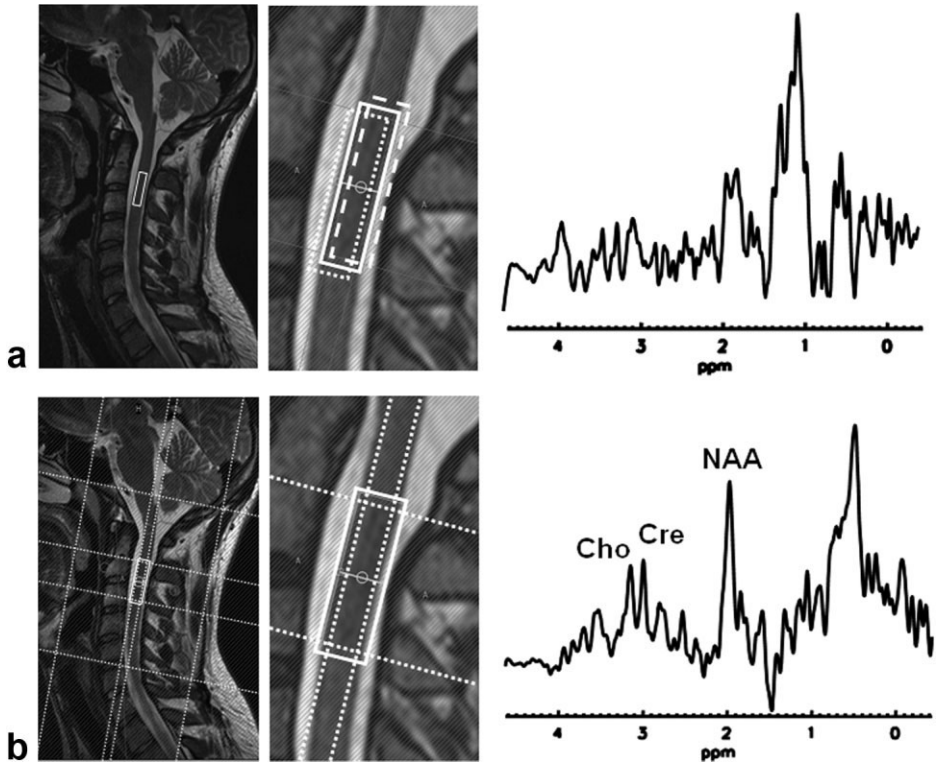

FIG. 1. **a:** Conventional PRESS localization (solid box) leads to chemical-shift displacement (dashed and dotted boxes) and therefore to lipid contamination and artifacts arising from pulsatile CSF flow and susceptibility differences. **b:** Enlargement of the PRESS box (solid box) and inner-volume saturation (dotted lines) based on the proposed PPR-based OVS has a significant impact on artifact reduction. Iterative first order shimming and F_0 determination was performed. No ECG triggering was used during the acquisition.

METHODS

Inner-Volume Saturation Based on RF Pulses With Polynomial Phase-Response

Inner-volume saturated PRESS localization (10) using six OVS bands based on highly selective, broadband RF pulses with Polynomial Phase-Response (13) was applied for single-voxel proton MRS in the spinal cord (Fig. 1). To account for the water-fat shift, 1.5-mm overprescription was applied. The frequency of excitation, refocusing, and saturation pulses was set to the NAA resonance. As described in detail by Henning et al. (12), for each geometrically described OVS band, two saturation pulses with flip angles, which have been numerically optimized for T_1-relaxation times of lipid (T_1 = 290 ms) and CSF (T_1 = 3120 ms), were utilized. Thus, T_1- and B_1-insensitive suppression of unwanted signal to below 3% of its original intensity was achieved. The maximum duration of each saturation pulse was 6 ms. To account for pulsatile CSF flow, which amounts up to 1 cm per cardiac cycle in the cervical spine (15), OVS slabs were not only placed anterior-posterior and right-left of the spectroscopy voxel but also along the head-feet direction. PPR pulses achieve bandwidths of 38.2 kHz, 12.3 kHz, or 6.2 kHz for flip angles of 30°, 90°, and 150°, respectively, for a maximum B_1 field strength of 13.5 μT (body coil—compare "experimental setup"). These large bandwidths enable high gradient strength and hence a negligible chemical shift displacement artifact (12,13). Fractional transition widths of 0.04 using PPR pulses with a normalized time-bandwidth product (nBW) of 500 (13) are sufficiently narrow for inner-volume suppression even combined with very small volume sizes as required in spinal cord spectroscopy (12,13). The OVS band thickness of 4 cm provides a good suppression of CSF and lipid signal. However, it compromises on the absolute fractional transition width of the saturation bands and, therefore, their selectivity. To avoid rephasing, amplitude and direction of spoiling gradients were periodically modulated following sinusoidal envelope functions that are shifted against each other in all three spatial dimensions (12,16–18).

Localized Shimming and F_0 Determination Based on Static Magnetic B_0 Mapping

Localized shimming and F_0 determination was based on high-resolution, cardiac-triggered static magnetic field B_0 mapping as described in detail by Schär et al. (14). B_0 maps were recorded in coronal direction with an in-plane and through-plane resolution of 2.1 mm. Up to 18 slices were acquired covering spinal cord, CSF and parts of the vertebral bodies in the region of interest. The shortest possible repetition time T_R of 9 ms and a difference in T_E of 2.3 ms were used for acquisition of the two necessary phase maps. The resulting B_0 maps were unwrapped prior to shim calculation if necessary. The calculation of optimal shim values to achieve field inhomogeneity corrections up to the second order was performed for a cylindrical volume around the MRS volume of interest, instead for the MRS volume itself (Fig. 2). This procedure avoids immediate transitions to inhomogeneous regions adjacent to the spectroscopy voxel due to the second order inhomogeneity correction. Therefore artifacts such as ghosting are obviated and better convergence of the shim optimization routine is achieved due to increased shim volume size. The optimization is based on a constraint Levenberg-Marquardt least-square minimization routine, aiming at fitting the linear and quadratic field terms, adjustable by the available shim coils, and thus correcting for the B_0 inhomogeneity distribution inside the selected shim volume.

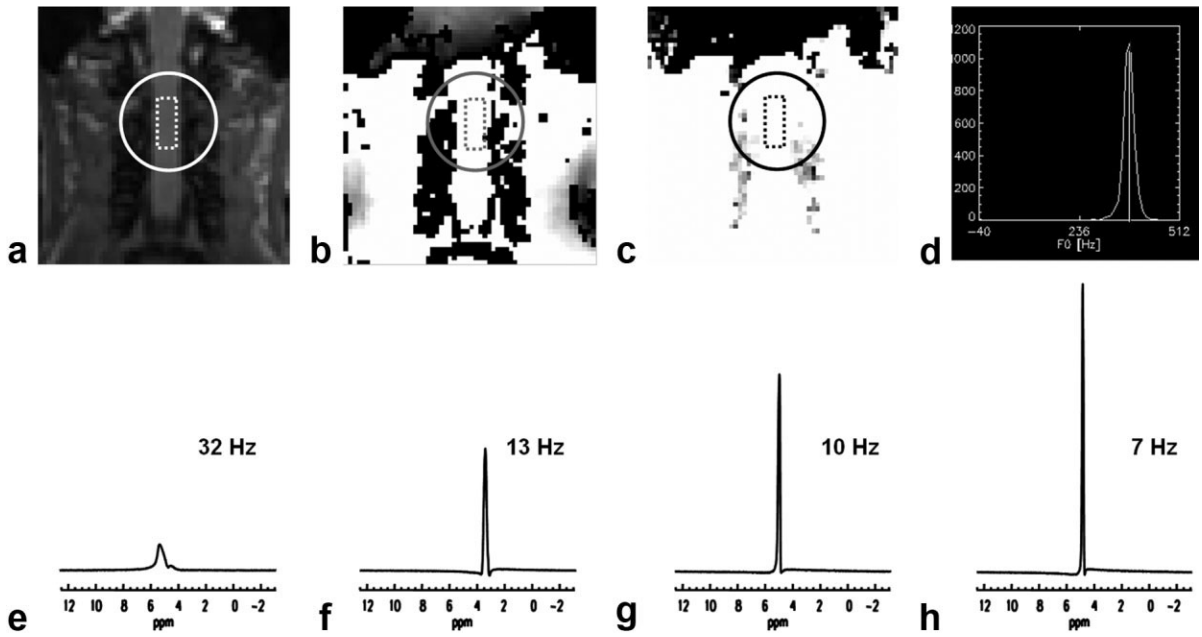

FIG. 2. Shimming based on static magnetic field B_0 mapping in the cervical spinal cord for a spectroscopy voxel (dotted line) at the C2-C3 level: shown are modulus image (**a**), initial B_0 map (pixels shown in black are masked and not used for the shim calculation) (**b**), inhomogeneity-corrected B_0 map (same threshold for masking) (**c**), and frequency distribution used for F_0 determination based on (c) inside the cylindrical shim volume (bold circle). Line width (FWHM) of unsuppressed water after first order iterative shimming (**e**), second order shimming based on B_0 mapping using the spectroscopy volume as shim volume (**f**), using a cylindrical volume as shim volume and a B_0 map acquired without (**g**) and with ECG triggering (**h**), are compared. ECG triggering and PPR-based OVS were applied for the MRS acquisitions.

Localized F_0 determination was performed subsequently by adding the calculated shim corrections to the initial B_0 map and determining the resonance frequency at the phase center of the selected shim volume. F_0 corrections were calculated in relation to the initially determined F_0 of the scout images, thus ensuring precise coregistration of planscan and spectroscopy voxel.

Experimental Setup

All MR experiments were performed on a Philips Achieva 3T scanner (Philips Medical Systems, Best, the Netherlands) using the integrated body-coil (maximum $B_1 = 13.5$ μT) for transmission and a Philips 12-element array spine coil for reception. Depending on the voxel location, two to four channels were combined for the MRS acquisition. ECG triggering with a trigger delay of 300 ms was performed to minimize motion artifacts, signal cancellation due to phase fluctuations, and to enhance shimming (2,19). In healthy volunteers, MRS voxel placement was aimed at minimization of the number of spanned spinal processes in order to further minimize B_0 distortions as suggested by Cooke et al. (2) (Fig. 1). This procedure has not always been applicable in patients since an adaptation of voxel size and position toward the lesion was necessary to avoid partial volume effects. Voxel sizes (unsaturated inner volume) were maximized depending on the size of the spinal cord or the lesion, respectively, and amounted to volumes between 0.36 ml and 1.49 ml, which correspond to dimensions of $4 \times 6 \times 15$ mm to $6.5 \times 8.5 \times 27$ mm. A high-resolution transversal T_2-weighted scout image was acquired to precisely plan the spectroscopy voxel. For the MRS acquisition, the minimum possible echo time (T_E) of 42 ms was used to maximize the SNR. A minimal repetition time of 2000 ms was used to reduce SNR loss due to saturation effects and to fulfill specific absorption rate (SAR) limitations. Due to ECG triggering, the actual repetition time depended on the individual heart rate and was slightly longer. For 512 averages a combined 16-step CYCLOPS (cyclically ordered phase sequence) and EXORCYCLE phase cycle was applied for artifact suppression. Depending on the actual heart rate, the total MRS scan time amounted to between 17 min and 21 min. Frequency locking (20) was switched off to avoid F_0 maladjustments during the scan arising from the limited signal intensity due to the small voxel sizes. For water suppression two chemical shift selective (CHESS) (21) pulses were applied prior to the OVS pulses. MRS data were quantified using LCModel (22,23) and a set of basis spectra simulated using GAMMA (http://www.nmr.ethz.ch/Gamma.html) including 20 metabolites such as NAA, Cho, Cre, mI, glutamate/glutamine (Glx), alanine (Ala), and lactate (Lac). Lipids (Lip) and macromolecules (MM) are simulated according to Seeger et al. (24) and included into the metabolite basis by default in LCModel (23). Metabolite concentrations based on fitting results with Cramer-Rao lower bounds (CRLB) smaller than 25% were considered in the quantitative analysis.

To test the influence of OVS on artifact suppression, ECG triggering was switched off, shimming and F_0 determination were based on conventional iterative methods.

For shimming tests inner-volume saturated PRESS localization and ECG triggering was used, but only 16 averages were acquired, since the line width of unsuppressed water was evaluated. All other measurements were performed according to the above description.

Volunteers and Patients

Sequence optimization was performed in 11 healthy volunteers. The finalized sequence was tested in eight healthy volunteers and three patients suffering from either an active demyelination in the spinal cord or a spinal cord tumor. Scout images, acquisition of a highly-resolved cardiac triggered B_0 map and calculation of shim settings, additional MRS preparation steps, and the MRS acquisition itself required 45 min to 1 h scan time. To minimize the time patients spent inside the MR scanner only one spectrum at the position of the lesion was acquired instead of recording an additional spectrum of adjacent healthy-appearing tissue. Spectra from healthy volunteers at the same position along the spinal cord were acquired instead for comparison.

RESULTS

Inner-Volume Saturation Based on RF Pulses With PPR

Comparative measurements in the cervical spinal cord at the C2-C3 level using PRESS localization without (Fig. 1a) and with inner-volume saturation based on PPR pulses (Fig. 1b) demonstrated the impact of OVS on artifact reduction and spectral quality enhancement. Since chemical-shift displacement (indicated by the dashed and dotted boxes around the solid box of the spectroscopy voxel in Fig. 1a) causes severe CSF contamination, spectra acquired using conventional PRESS localization revealed artifacts and SNR loss caused by signal cancellation due to phase fluctuations. While the most prominent peaks visible in neuronal tissue NAA, Cho, and Cre were not assignable, resonances at macromolecule and lipid frequencies were predominant in that case (Fig. 1a). The use of the proposed inner-volume saturation scheme enhanced the spectral quality significantly (enlarged solid box indicates the spectroscopy volume and the dotted lines the borders of the OVS bands in Fig. 1b). NAA, Glx, Cre, Cho, and mI could be clearly assigned (Fig. 1b). The remaining lipid/MM resonances indicated a dislocation problem of the excited volume due to F_0 misdetermination using conventional iterative shimming and F_0 determination.

Localized Shimming and F_0 Determination Based on Static Magnetic B_0 Mapping

The proposed second-order shimming algorithm based on static magnetic field B_0 mapping (Fig. 2a–d) was compared to localized iterative first-order shimming and to localized second-order shimming based on the FASTERMAP algorithm (25,26). In order to clearly resolve resonances and increase the peak amplitude to achieve a sufficient SNR, a B_0 inhomogeneity correction leading to a water line width (FWHM, unsuppressed) of 12 Hz or below is necessary. Both FASTERMAP and iterative shim showed only sporadic convergence toward this criterion at the C2-C3 level, in about one out of six volunteers and did hardly ever converge at lower levels along the spinal cord. The proposed localized shim based on static magnetic B_0 mapping did converge in all measured volunteers in the upper and medium cervical spinal cord down to the C5 level toward the above mentioned criterion and even showed improved performance as compared to the two alternative methods further along the thoracic spinal cord caudally. Figure 2 demonstrates the typical enhancement of inhomogeneity correction and therefore water line width at the C2-C3 level using B_0 mapping compared to iterative shimming. Best convergence of inhomogeneity correction and F_0 determination was achieved when the shim volume was cylindrical with a diameter of about the double voxel size centered at the position of the spectroscopy volume rather than a voxel-sized box or a larger shim volume (Fig. 2f and g). Further improvement was attained by using ECG triggering during the acquisition of the B_0 map (Fig. 2h). The described localized F_0 determination based on the inhomogeneity corrected B_0 map (Fig. 2d) enabled precise coregistration of the spectroscopy voxel with the scout image. Hence, the combination of OVS and localized F_0 determination effectively prevented lipid contamination stemming from the surrounding epidural, muscle and subcutaneous fatty tissue (Fig. 3).

ECG Triggering

Measurements performed on three healthy volunteers at the C2-C3 level with and without ECG triggering proved that the line width of the unsuppressed water signal increases significantly from 8 Hz to up to 15 Hz when ECG triggering is switched off. This is in accordance with findings of Cooke et al (2).

MRS in the Cervical Spine

Reproducible shim convergence and precise localization extended the applicability of quantitative MRS to the entire cervical spinal cord (Figs. 3 and 4). Unambiguous resonance assignments and LCModel-based quantification was achieved in the upper (Fig. 3a) as well as in the medium and lower cervical spine (Fig. 3b). Average metabolite concentration ratios from eight healthy volunteers measured at different levels along the cervical spinal cord were in accordance with earlier findings (Table 1) (2,3). While NAA, Cho, and Cre concentrations show a low intersubject variability and hence indicate precise quantification, the determined Glx and mI concentrations vary significantly. As illustrated in Fig. 4, the proposed measurement protocol also allowed for the acquisition of sound spectra from spinal cord lesions in the entire cervical spine, even if their inhomogeneity introduced further artifact sources (Fig. 4a). Metabolite concentration ratios in individual patients were clearly distinct compared to the average values of healthy subjects and reveal similar trends as reported previously for the brain (Table 1) (27). Detection of pathologic Lac was possible. Macromolecule resonances are visible in both patient spectra at around 1.5 ppm (Fig. 4) (27,28), but have significant contributions from modulation side bands (29,30) as indicated by an-

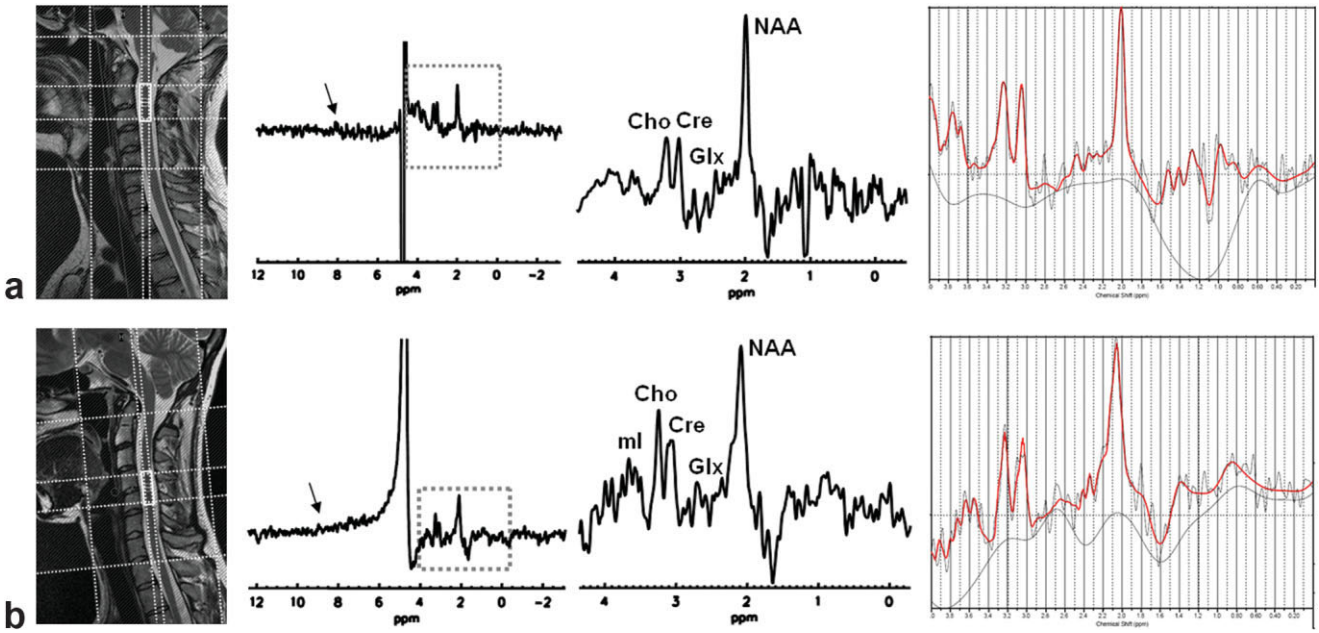

FIG. 3. Representative spectral quality and LCModel fitting results (see Table 1) at the C2-C3 (**a**) and the C4-C5 (**b**) level, which were reproducibly achieved in eight healthy volunteers at different levels along the cervical spine using ECG triggering, inner-volume saturation based on PPR pulses as well as shimming and F_0 determination based on static magnetic field B_0 mapping (T_E = 42 ms, T_R = 2000 ms, 512 averages). The arrows indicate modulation sidebands.

tiphase peaks at the same distance in Hz downfield of the water (compare Fig. 3).

MRS in the Thoracic and Lumbar Spine

In contrast to the cervical spinal cord, sufficient shim convergence could not be reached in the thoracic and lumbar spinal cord of healthy volunteers (Fig. 5). This is probably due to more complex CSF flow pattern, spinal cord movement, and the smaller dimensions of the thoracic cord. Resulting water line widths using the proposed shimming, F_0 determination, and acquisition scheme indicate that inhomogeneity correction is especially difficult

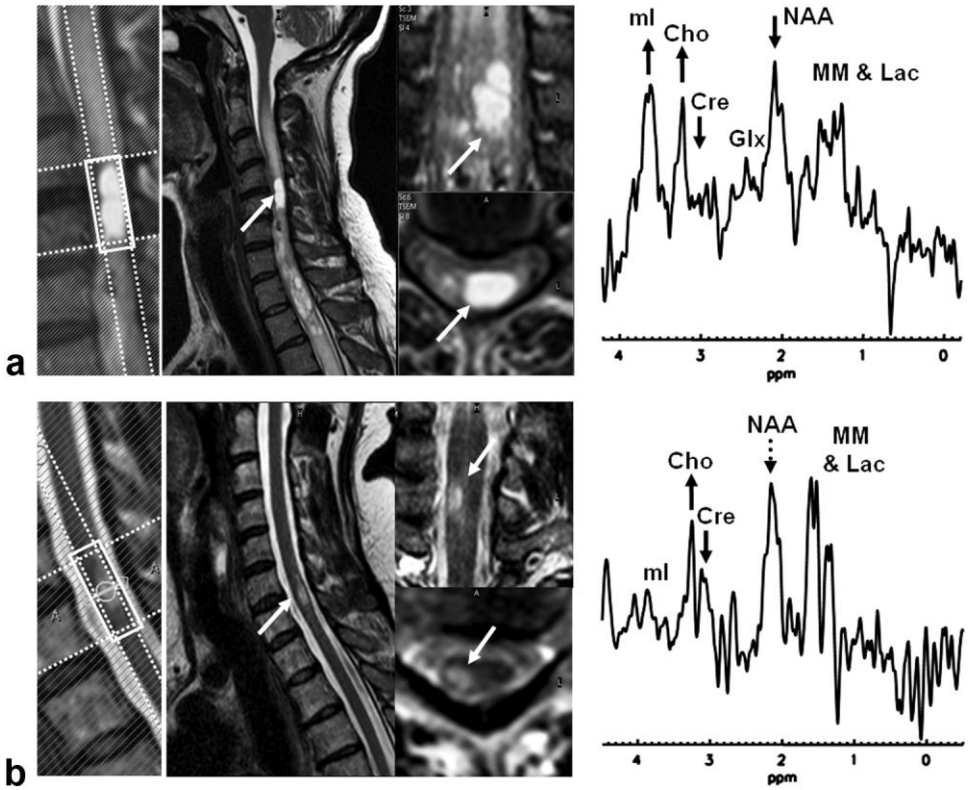

FIG. 4. Spinal cord MR spectra (T_E = 42 ms, T_R = 2000 ms, 512 averages) acquired in a patient with an intramedullary tumor at the C4-C5 level (**a**) and a patient with an active demyelinating lesion due to multiple sclerosis at the C6-C7 level (**b**). Compared to the average metabolite concentrations determined in healthy volunteers a decrease of NAA and Cre as well as an increase of Choline, ml, and Lac are observable in the tumor patient (a; Table 1). In the MS patient a decrease of NAA and Cre as well as an increase of Choline and Lac are detected (b; Table 1). Modulation sidebands contribute to the MM resonance at about 1.5 ppm. ECG triggering, PPR-based OVS, and shimming as well as F_0 determination based on static magnetic field B_0 mapping were applied.

Table 1
Relative metabolite concentrations in the cervical spine of eight healthy volunteers (mean ± SD, different levels C1-C2 to C6-C7) and three Individual patient cases Indicate the diagnostic value of quantitative spinal cord MRS.

	NAA/Cre	NAA/Cho	Cho/Cre	mI/Cre	Glx/Cre	Lac/Cre
Healthy volunteers cervical spine	1.22 ± 0.06	4.9 ± 1.3	0.27 ± 0.08	1.4 ± 0.6	2.1 ± 0.7	x
Tumor C 4/5	1.86	1.9	0.97	12.9	1.9	4.7
Demyelination C 6/7	0.68	1	0.68	0.7	x	0.9
Tumor Th 9[a]	0.47	1.1	0.42	1	2.3	x

[a]T_E = 144 ms instead of 42 ms as for all other measurements.
x = no reliable quantification result.

in the thoracic spinal cord, while shim convergence improves again in the lumbar spine. However, in the thoracic spinal cord at the T9 level, sufficient shimming (12 Hz unsuppressed water line width at FWHM) and hence a quantifiable spectral quality was achieved in a patient with an intramedullary space-occupying lesion, which obliterates the adjacent subarachnoid space and hence significantly reduces pulsatile CSF flow and movements of the spinal cord due to its dimensions (Fig. 6). No modulation sidebands obscured the spectrum (29,30). Detected changes comprise Cho, Glx, and MM increase as well as NAA decrease.

DISCUSSION

Impact of Methodological Advances on Artifact Suppression

Inner-volume saturated PRESS (10) using highly selective T_1- and B_1-insensitive OVS based on broadband PPR pulses (12,13) minimizes chemical shift displacement. Thus lipid contamination and anomalous J-modulation are diminished. Hence pathologic Lac detection is enabled. In addition, SNR increase and correct metabolite ratios are achieved, since inner-volume saturation ensures the same effective voxel size inside the spinal cord for all metabolites. CSF flow artifacts such as signal cancellation due to phase fluctuations and ghosting are significantly reduced by saturating inflowing CSF by OVS slabs above and below the spectroscopy volume and ensuring precise voxel localization along the border between CSF and neural tissue in anterior-posterior and left-right direction. Both highly selective, broadband PPR pulses (13) and numerical flip angle optimization (12) are prerequisites for the use of inner-volume suppression in spinal cord MR spectroscopy. A very narrow fractional transition width is required to avoid suppression of desired signal due to the small voxel size. Considering the close proximity of CSF, bone, muscle, and subcutaneous fat tissue, robust simultaneous suppression of lipid and CSF signal is additionally needed. The latter requires broadband saturation pulses, which allow for high gradient strength and therefore a minimal water-fat shift, as well as T_1- and B_1-insensitivity of the OVS, which is enabled by the use of two OVS cycles and numerical flip angle optimization (12). Disadvantages of the inner-volume saturation sequence are a slight scan time prolongation and the occurrence of water modulation side bands (29,30) due to the prolonged delay between water suppression pulse and excitation pulse. The former is unavoidable, since a minimal repetition time of 2000 ms has to be used to fulfil specific absorption rate restrictions. On the other hand, this prevents additional SNR loss due to saturation effects. The latter might be significantly improved using an interleaved VAPOR (variable power RF pulses with optimized relaxation delays) (31) and OVS scheme. Alternative approaches are the consideration of the modulation sidebands during postprocessing and quantification (29) or the use of two acquisitions with inverted gradients (30).

High-quality inhomogeneity corrections, and therefore narrow resonance lines, are crucial to achieve sufficient SNR and an interpretable spectral quality using small voxel sizes as required for MRS in the spinal cord. Hence, reproducible shim convergence is a prerequisite for the successful use of spinal cord spectroscopy in physiological studies or clinical diagnostics. The proposed localized shimming and F_0 determination method based on static magnetic B_0 mapping fulfils the reproducibility requirement. It proves to be superior to iterative shimming and FASTERMAP in the presence of strong susceptibility differences as well as increased flow and motion adjacent to the volume of interest, as in the case of the spinal cord. This has also been demonstrated in previous MRI studies of the myocardium (14). Precise F_0 determination and correction relative to the F_0 of the scout image enables correct coregistration of the spectroscopy voxel. Hence lipid contamination is avoided and SNR maximized. However, the acquisition of the cardiac triggered B_0 map and the offline determination of shim currents and F_0 correction values prolongs the overall scan protocol significantly.

Extended Applicability and Diagnostic Value of Spinal Cord MRS

The proposed combination of ECG triggering, inner-volume saturation, and localized shimming and F_0 determination improves both the quality and consistency of the spectra. In contrast to all previous quantitative spinal cord MRS studies, which were limited to the upper cervical spine down to the C2-C3 level (2–6), the proposed measurement protocol allows for quantitative analysis of MRS data from the entire cervical spinal cord even in inhomogeneous lesions. To clarify whether metabolite concentrations change along the healthy cervical spinal cord, further studies including larger groups of volunteers are needed. The comparison of patient spectra with spectra from healthy volunteers demonstrates the potential clinical use of spinal cord spectroscopy. In comparison with corresponding brain lesions, similar trends of metabolite concentration changes are detected (27,28), while absolute concentrations might significantly differ between patholo-

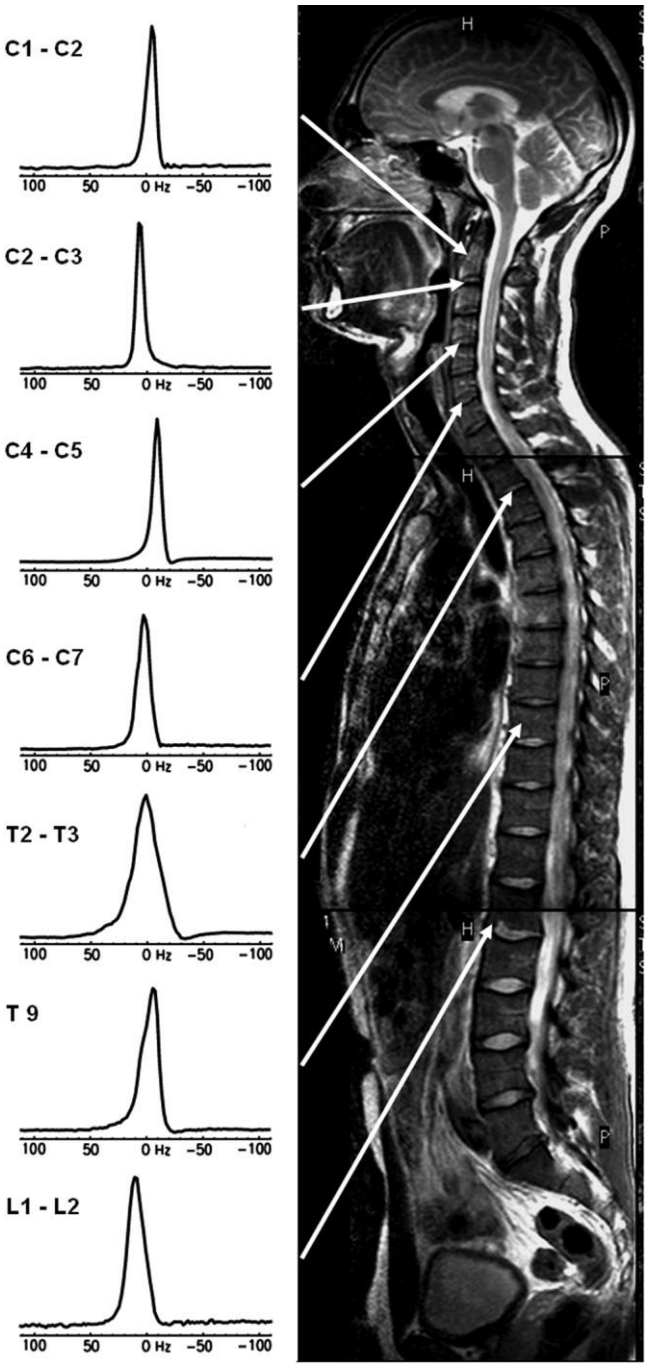

FIG. 5. Shim quality in healthy volunteers along the spinal cord. Line width (FWHM) of unsuppressed water at the level of C1-C2 = 8 ± 1 Hz (N = 3), C2-C3 = 8 ± 2 Hz (N = 5), C4-C5 = 10 Hz (N = 1), C6-C7 = 14 ± 2 Hz (N = 3), T2-T3 = 25 Hz (N = 1), T9 = 25 ± 5 Hz (N = 3), and L1-L2 = 22 ± 3 (N = 3) (mean ± SD for $N \geq 3$).

gies in brain and spinal cord. However, identification of pathology specific changes in spectral pattern for disorders such as demyelination or certain tumors requires studies with larger patient groups. Earlier MRS studies in spinal cord lesions of multiple sclerosis and tumor patients either suffered from poor spectral quality (9) or lack of quantification (8).

High-quality MRS data from a patient with a space-occupying intramedullary tumor in the lower thoracic spinal cord, which occluded almost the entire spinal canal and therefore hindered CSF flow, were obtained using inner-volume saturation and advanced shimming, but no ECG triggering. This demonstrates that susceptibility problems introduced by the lung are not of vital importance for obtaining successful MRS in the thoracic spinal cord. However, shim convergence in healthy volunteers was insufficient in this anatomical region. Hence, the source of artifacts and shim problems in the thoracic cord is most likely CSF flow induced by respiratory motion. It was demonstrated by Cooke et al. (2) and our own work that ECG triggering efficiently compensates for CSF flow and the resulting movement of the spinal cord induced by cardiac motion and thus significantly improves shimming and spectral quality in the cervical spine. According to Friese et al. (32,33), further caudally in the thoracic and lumbar spine CSF flow is additionally induced by respiratory motion, whereas the influence of cardiac motion is decreasing. Additional CSF flow compensation using techniques such as respiratory gating, navigator gating, and volume tracking (34–37) is most likely a prerequisite for the general extension of spinal cord MRS to the thoracic spinal cord. Shim convergence improves again in the lumbar spinal cord, where CSF flow is significantly decreased in comparison to cervical and thoracic spinal cord, while the flow pattern is more complex (15). Examples of interpretable MRS data in the conus medullaris and in patients with large intramedullary lesions in the lumbar region occluding the spinal canal have been reported by Dydak et al. (7) and by Kim et al. (8). However, the small size of the lumbar spinal cord (although its diameter is larger than the thoracic cord, it is still smaller than in the cervical region) and its large degree of freedom with respect to motion limit the applicability of spinal cord MRS in that area. Considering the propagation of the pulsatile blood flow during one cardiac cycle the moment of peak CSF flow depends on its position along the spinal canal (32,33). Hence a separate adjustment of the ECG trigger delay depending on the spinal cord level might be necessary (19). The impact of pulsatile CSF flow might be further reduced by storing each individual phase cycle separately, which allows for sorting out spectra with motion artifacts and averaging only the remaining artifact free, individually postprocessed spectra, as suggested by Tkac et al. (38). Furthermore, SNR might be significantly increased by the use of dedicated spinal cord spectroscopy RF coils (39–40).

CONCLUSIONS

In conclusion, the proposed combination of ECG triggering, inner-volume saturation based on a numerically optimized OVS utilizing broadband, highly selective PPR pulses as well as localized shimming, and F_0 determination based on static magnetic field B_0 mapping, extends the applicability of quantitative MRS to the entire length of the cervical spinal cord. In this anatomical region, quantitative metabolic information of the healthy spinal cord as well as spinal cord lesions can be assessed. Furthermore, examination of edematous or space-occupying lesions, which fill the spinal canal thus reducing CSF flow and

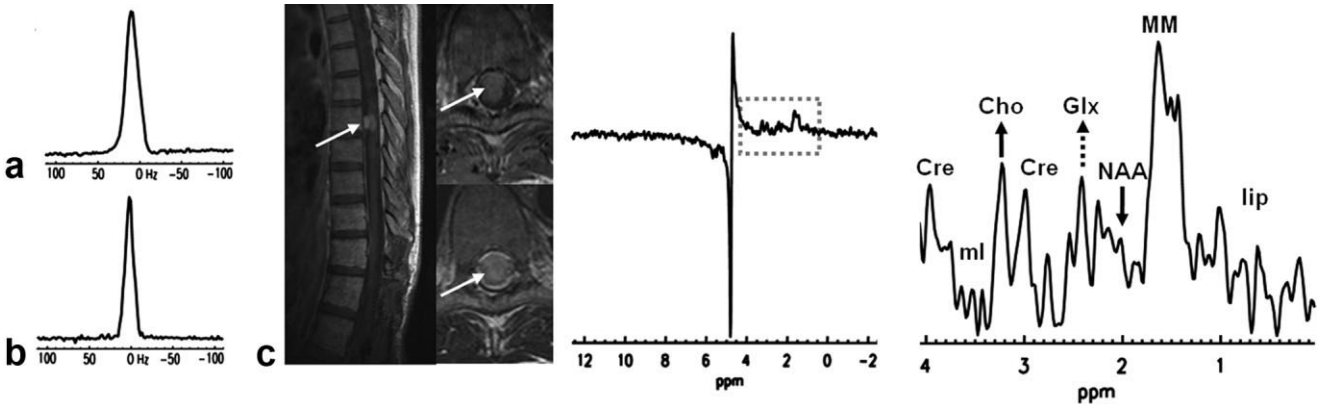

FIG. 6. Shim quality at the T9 level in a healthy volunteer (**a**) and a patient with a space-occupying intramedullary lesion, which occludes the entire spinal cord canal (**b**,**c**). Line width (FWHM) of unsuppressed water in healthy volunteers amounts to 25 ± 5 Hz ($N = 3$), leading to an undesirable spectral quality. In the patient a much better line width of 12 Hz could be achieved, which enabled the acquisition of a quantifiable spinal cord MR spectrum at the T9 level ($T_E = 144$ ms, $T_R = 2000$ ms, 512 averages) (c). Compared to the average metabolite concentrations determined in healthy volunteers, a decrease of NAA as well as an increase of Choline and Glutamate, is observed (Table 1). No modulation sidebands were detected. Thus the resonance at about 1.5 ppm was tentatively assigned to MM. No ECG triggering was used. PPR-based OVS as well as iterative shimming and F_0 determination were applied.

cord movements, are possible along the entire spinal cord, including lower thoracic and lumbar segments.

ACKNOWLEDGMENTS

We thank Roger Luechinger for professional technical and information technology support and Michaela Soellinger for helpful discussions on pulsatile CSF flow. Supported in part by National Centers of Competence in Research (NCCR) on Neural Plasticity and Repair (to S.S.K.).

REFERENCES

1. Lin A, Ross BD, Harris K, Wong W. Efficacy of proton magnetic resonance spectroscopy in neurological diagnosis and neurotherapeutic decision making. NeuroRx 2005;2:197–214.
2. Cooke FJ, Blamire AM, Manners DN, Styles P, Rajagopalan B. Quantitative proton magnetic resonance spectroscopy of the cervical spinal cord. Magn Reson Med 2004;51:1122–1128.
3. Marliani AF, Clementi V, Albini-Riccioli L, Agati R, Leonardi M. Quantitative proton magnetic resonance spectroscopy of the human cervical spinal cord at 3 Tesla. Magn Reson Med 2007;57:160–163.
4. Gomez-Anson B, MacManus DG, Parker GJ, Davie CA, Barker GJ, Moseley IF, McDonald WI, Miller DH. In vivo 1H-magnetic resonance spectroscopy of the spinal cord in humans. Neuroradiology 2000;42:515–517.
5. Blamire AM, Cader S, Lee M, Palace J, Matthews PM. Axonal damage in the spinal cord of multiple sclerosis patients detected by magnetic resonance spectroscopy. Magn Reson Med 2007;58:880–885.
6. Edden RA, Bonekamp D, Smith MA, Dubey P, Barker PB. Proton MR spectroscopic imaging of the medulla and cervical spinal cord. J Magn Reson Imaging 2007;26:1101–1105.
7. Dydak U, Kollias SS, Schär M, Meier D, Boesiger P. MR spectroscopy in different regions of the spinal cord and in spinal cord tumors. In: Proceedings of the 13th Annual Meeting of ISMRM, Miami Beach, FL, USA, 2005 (Abstract 813).
8. Kim YG, Choi GH, Kim DH, Kim YD, Kang YK, Kim JK. In vivo proton magnetic resonance spectroscopy of human spinal mass lesions. J Spinal Disord Tech 2004;17:405–411.
9. Kendi AT, Tan FU, Kendi M, Yilmaz S, Huvaj S, Tellioglu S. MR spectroscopy of cervical spinal cord in patients with multiple sclerosis. Neuroradiology 2004;46:764–769.
10. Edden RA, Schär M, Hillis AE, Barker PB. Optimized detection of lactate at high fields using inner volume saturation. Magn Reson Med 2006;56:912–917.
11. Kreis R. Issues of spectral quality in clinical ^{1}H-magnetic resonance spectroscopy and a gallery of artifacts. NMR Biomed 2004;17:361–381.
12. Henning A, Schär M, Schulte RF, Wilm B, Pruessmann KP, Boesiger P. SELOVS: brain MRSI localization based on highly selective T_1- and B_1-insensitive outer-volume suppression at 3T. Magn Reson Med 2008; 59:40–51.
13. Schulte RF, Henning A, Tsao J, Boesiger P, Pruessmann KP. Design of broadband RF pulses with polynomial phase response. J Magn Reson 2007;186:167–175.
14. Schär M, Kozerke S, Fischer SE, Boesiger P. Cardiac SSFP imaging at 3 Tesla. Magn Reson Med 2004;51:799–806.
15. Friese S, Klose U, Voigt K. Zur Pulsation des Liquor cerebrospinalis. Klin Neuroradiol 2002;12:67–75.
16. Chu A, Alger JR, Moore GJ, Posse S. Proton echo-planar spectroscopic imaging with highly effective outer volume suppression using combined presaturation and spatially selective echo dephasing. Magn Reson Med 2003;49:817–821.
17. Günther M, Feinberg DA. Simultaneous spin echo refocusing. Magn Reson Med 2005;54:513–523.
18. Luo Y, de Graaf RA, DelaBarre L, Tannus A, Garwood M. BISTRO: an outer-volume suppression method that tolerates RF field inhomogeneity. Magn Reson Med 2001;45:1095–1102.
19. Summers P, Staempfli P, Jaermann T, Kwiecinski S, Kollias S. Impact of trigger timing on diffusion tensor imaging of the human spinal cord. AJNR Am J Neuroradiol 2006;27:1952–1961.
20. Henry PG, van de Moortele PF, Giacomini E, Nauerth A, Bloch G. Field-frequency locked in vivo proton MRS on a whole-body spectrometer. Magn Reson Med 1999;42:636–642.
21. Haase A, Frahm J, Hanicke W, Matthaei D. ^{1}H NMR chemical shift selective (CHESS) imaging. Phys Med Biol 1985;30:341–344.
22. Provencher SW. Estimation of metabolite concentrations from localized in vivo proton NMR spectra. Magn Reson Med 1993;30:672–679.
23. Provencher SW. LCModel manual. http://www.s-provencher.com/pages/lcmodel.shtml.
24. Seeger U, Klose U, Mader I, Grodd W, Nägele T. Parameterized evaluation of macromolecules and lipids in proton MR spectroscopy of brain diseases. Magn Reson Med 2003;49:19–28.
25. Gruetter R, Boesch C. Automatic, localized in vivo adjustment of all first and second order shim coils. J Magn Reson 1992;96:323–334.
26. Shen J, Rycyna RE, Rothman DL. Improvements on an in vivo automatic shimming method (FASTERMAP). Magn Reson Med 1997;38: 834–839.

27. Brandao LA. MR spectroscopy of the brain. Philadelphia: Lippincott Williams & Wilkins; 2004.
28. Mader I, Seeger U, Weissert R, Klose U, Naegele T, Melms A, Grodd W. Proton MR spectroscopy with metabolite-nulling reveals elevated macromolecules in acute multiple sclerosis. Brain 2001;124:953–961.
29. Serrai H, Clayton DB, Senhadji L, Zuo C, Lenkinski RE. Localized proton spectroscopy without water suppression: removal of gradient induced frequency modulations by modulus signal selection. J Magn Reson 2002;154:53–59.
30. Dong Z, Dreher W, Leibfritz D. An experimental method to eliminate frequency modulation sidebands in localized in vivo ^{1}H MR spectra acquired without water suppression. Magn Reson Med 2004;51:602–606.
31. Tkac I, Starcuk Z, Choi IY, Gruetter R. In vivo ^{1}H NMR spectroscopy of rat brain at 1 ms echo time. Magn Reson Med 1999;41:649–659.
32. Friese S, Hamhaber U, Erb M, Kueker W, Klose U. The influence of pulse and respiration on spinal cerebrospinal fluid pulsation. Invest Radiol 2004;39:120–130.
33. Friese S, Hamhaber U, Erb M, Klose U. B-waves in cerebral and spinal cerebrospinal fluid pulsation measurement by magnetic resonance imaging. J Comput Assist Tomogr 2004;28:255–262.
34. Wang Y, Rossmann PJ, Grimm RC, Riederer SJ, Ehman RL. Navigator-echo-based real-time respiratory gating and triggering for reduction of respiratory effects in three-dimensional coronary MR angiography. Radiology 1996;198:55–60.
35. Tyszka JM, Silverman JM. Navigated single-voxel proton spectroscopy of the human liver. Magn Reson Med 1998;39:1–5.
36. Kozerke S, Schär M, Lamb HJ, Boesiger P. Volume tracking cardiac ^{31}P spectroscopy. Magn Reson Med 2002;48:380–384.
37. Schär M, Kozerke S, Boesiger P. Navigator gating and volume tracking for double-triggered cardiac proton spectroscopy at 3 Tesla. Magn Reson Med 2004;51:1091–1095.
38. Tkac I, Andersen P, Adriany G, Merkle H, Ugurbil K, Gruetter R. In vivo ^{1}H NMR spectroscopy of the human brain at 7T. Magn Reson Med 2001;46:451–456.
39. Buehrer M, Huber ME, Wiesinger F, Boesiger P, Kozerke S. Coil-setup optimization for 2D-SENSE whole-heart coronary imaging. Magn Reson Med 2006;55:460–464.
40. Massner JA, Staempfli PWM, De Zanche N, Kozerke S, Pruessmann KP. DTI and fiber tracking of the median nerve using an adjustable wrist coil array. In: Proceedings of the 15th Annual Meeting of ISMRM, Berlin, Germany, 2007 (Abstract 80).